A Demonstration of Precise Calibration of Tropospheric Delay Fluctuations With Water Vapor Radiometers

L. P. Teitelbaum, R. P. Linfield, and G. M. Resch
Tracking Systems and Applications Section

S. J. Keihm and M. J. Mahoney
Microwave, Lidar, and Interferometer Technology Section

An advanced water vapor radiometer (WVR), currently under development in the DSN Technology Program, will serve as the critical remote sensing instrument in the troposphere calibration subsystem required by the Cassini radio science experiments. The ability of WVRs to calibrate changes in tropospheric delay was demonstrated during very long baseline interferometry (VLBI) observations on the 21-km baseline between DSS 13 and DSS 15 at Goldstone, California. WVR measurements reduced the observed VLBI post-fit delay residuals over a 13-h period from 43.8 ps to 16.9 ps, a factor of ≈2.5. When applied to shorter time intervals, an ≈50-percent reduction in the Allan standard deviation of the site-differenced residual delay on 100- to 700-s time scales was achieved during conditions of high tropospheric activity. Thermal WVR noise precluded calibration of delay fluctuations on shorter time scales and during quiet tropospheric conditions.

I. Introduction

The main objective of a very long baseline interferometry (VLBI) observation of a compact natural radio source is to estimate the geometric delay, the relative delay in arrival time of a wave front from the source at two widely separated antennas, from which the angular position of the source on the sky can be accurately determined. Similarly, the objective of a Doppler tracking measurement of a spacecraft is to estimate the geometric delay rate, the time rate of change of the round-trip tracking signal delay between the spacecraft and a single antenna, from which the radial velocity of the spacecraft can be found. The geometric delay or delay rate is that which would be measured if perfect instrumentation detected signals traveling through vacuum between the signal source and the Earth. Radio science experiments infer phenomena of physical interest, for example, the structure of a planetary atmosphere or evidence for the passage of a gravitational wave, by measuring perturbations to the geometric delay along a spacecraft tracking link. However, nongeometric effects that corrupt the measurements must first be removed from the data, either by modeling and estimation or by direct calibration. For measurements that are insensitive to the effects of ionized media, such as high single-frequency ($\nu \gtrsim 20$ GHz) Doppler or dual-frequency VLBI, nondispersive tropospheric effects will dominate the media contribution to the signal. As an example, although a mean tropospheric delay usually can be estimated from the data, stochastic tropospheric fluctuations about the mean have substantial power over a wide range of time scales [10].

Measurements at 32 GHz of the two-way phase between Earth and the Cassini spacecraft during its cruise to Saturn will be used to search for low-frequency (10^{-4} to 10^{-2} Hz) gravitational radiation. The sensitivity of the search will be limited by our ability to calibrate the tropospheric delay on the uplink and downlink signals. Because most of the power in tropospheric delay fluctuations at frequencies <0.01 Hz is believed to be due to fluctuations in water vapor density [4], efforts at calibrating these *wet* delay fluctuations have focused on the use of water vapor radiometers (WVRs) [3]. An advanced WVR, currently under development, will serve as the critical remote sensing instrument in the troposphere calibration subsystem required to support Cassini radio science.

VLBI/WVR comparison experiments on the 21-km baseline between DSS 13 and DSS 15 provide a way to validate the WVR calibration concept. A short-baseline VLBI experiment isolates wet delay fluctuations because most delay errors cancel or are negligible on baselines $\lesssim$200 km. The VLBI delay residuals (i.e., after subtraction of an accurate model) will be dominated by unmodeled delay variations in the wet troposphere. A previous attempt to calibrate delay fluctuations with WVRs [7] was only marginally successful, due to quiet tropospheric conditions and difficulties with instrumentation at one radio antenna. However, the present experiment convincingly demonstrates the ability of current generation WVRs to precisely measure short time-scale path delay fluctuations and to provide a calibration that dramatically reduces the impact of unmodeled, tropospheric delay variations on VLBI observations.

II. Observations and Data Reduction

From September 10 through 11, 1994, at Goldstone, California, we conducted dual-frequency (2.3- and 8.4-GHz) VLBI observations on the 21-km baseline between two of NASA's Deep Space Network (DSN) 34-m-diameter antennas, a new beam-waveguide antenna at DSS 13, and a high-efficiency antenna at DSS 15. In order to reduce tropospheric sampling differences due to beam offset, WVRs [5][1] were positioned approximately 50 m from each DSN antenna, the minimum separation that still allowed a clear WVR field of view. These short baseline measurements took place during an intercontinental VLBI experiment. We therefore used a schedule optimized for long-baseline astrometry, including frequent low elevation angle measurements down to the VLBI horizon at $\theta = 6$ deg. Because the WVRs had large conical beams of width ~6–9 deg full width, half maximum (FWHM), a WVR horizon was imposed at $\theta = 30$ deg to avoid ground pickup. The WVRs do not track sidereally and were pointed at the mean elevation and azimuth angles during each scan.

There were 175 scans, spanning 15 hours. All scans were from 110 to 160 s in duration, except for three long scans that were $\approx$2000 s in length. The long scans were scheduled at high elevation angles, $\theta > 40$ deg, which assured that WVR copointing was possible. They were also timed to occur near source meridian transit, which minimized changes in elevation angle during the scans. These would introduce systematic delay trends in the VLBI data due to changing path length through the mean troposphere. This experimental setup was nearly identical to that of our previous observations [7]. Weather conditions were warm and clear.

Formatted data streams from both DSN antennas were cross-correlated in real time. The correlator output was processed with astrometric and geodetic data reduction software. Fringe fitting estimated one group delay and phase delay rate for each scan, for each of the two frequency bands, and also yielded a time series of interferometer residual phases with respect to the fitted phase model. Bright sources were selected for the long scans so that a precise residual phase could be extracted every 2 s. A linear combination of the observables from each frequency band was formed, which removed the effect of charged particles in the ionosphere and interplanetary medium. The charged particle-free group delays were used as input observables to a multiparameter estimation step that extracted model parameters, such as those

[1] S. J. Keihm, *Water Vapor Radiometer Intercomparison Experiment: Platteville, Colorado, March 1–14, 1991*, JPL D-8898 (internal document), Jet Propulsion Laboratory, Pasadena, California, 1991.

characterizing a site-differenced linear clock and a site-differenced zenith troposphere delay. The scan-to-scan residuals with respect to the model are expected to be dominated by unmodeled tropospheric fluctuations about the average, site-differenced, zenith troposphere estimated from the data.

WVR output voltages were converted to brightness temperatures using gains estimated by the tip curve method [11]. Brightness temperatures were converted to path delays using linear retrieval coefficients determined from model calculations based on radiosonde data [11]. Although both WVRs were two-channel instruments, all results reported here used only the lower noise, vapor-sensing channel at 20.7 GHz, sufficient under the clear conditions of our observations. A line-of-sight (LOS) path delay was estimated for each WVR every ∼6 s. A number of scans were lost to data acquisition failures of either the VLBI or WVRs. Scans were also rejected if the WVR brightness temperatures exhibited evidence of ground pickup or contamination from radio emission from the Sun, or if the VLBI post-fit residuals were clear outliers in the full experiment solution. The full, valid data set consisted of 80 scans. When the WVRs were forced to point at higher elevation angles θ_W than the DSN antennas, because the scheduled source fell below the WVR horizon at $\theta = 30$ deg, estimates of the LOS delays were determined by assuming that LOS path delays $\tau(\theta)$ were related to WVR-derived path delays $\tau_W(\theta_W)$ by the mapping function $\tau(\theta) = \tau_W(\theta_W) \sin\theta_W / \sin\theta$. A subset of the valid data for which the WVR and VLBI antennas were copointed to within 1 deg at both ends of the baseline consisted of 30 scans. A more detailed description of the data reduction can be found in [7].

III. Results and Discussion

The time series of the site-differenced (DSS 13–DSS 15) LOS phase delay residuals for two long scans for the VLBI and WVR data are shown in Fig. 1. The VLBI phase delays τ are determined every 2 s from the measured interferometer residual phase. A linear trend has been subtracted from the VLBI data during fringe fitting [8], removing any clock-like effects. To ensure comparable treatment of the WVR data, the path delay time series of each WVR has had an equivalent linear model estimated and removed. This is important because at a fixed elevation angle a site-differenced, tropospheric delay that varies linearly with time is indistinguishable from a linearly drifting clock. Because both the time-tagging and the data acquisition duty cycles are different for each WVR, the WVR residual delays have been linearly interpolated at 6-s intervals, coinciding with every third VLBI residual delay delivered by the correlator.

Both plots exhibit strong correlations between the VLBI and WVR time series over the full ∼2000-s time scale, especially scan 93, which has much larger delay variations. Scan 20 occurred at 9 a.m. local time, before the development of large-scale convection in the lower troposphere. In contrast, scan 93 occurred at 3 p.m. local time, near the peak of large-scale, turbulent convection.

The rms of the delay variations in Fig. 1 are summarized in Table 1 for the VLBI and WVR data separately and for the differenced time series (not plotted) $\Delta(t) \equiv \mathrm{VLBI}(t) - \mathrm{WVR}(t)$. Also shown are estimates of the tropospheric volume sampling error σ_{beam} (the expected rms delay difference due to WVR/VLBI antenna beam offset,WVR/VLBI antenna beam mismatch, and WVR nonsidereal tracking) and Δ^*, the rms of the differenced time series after subtraction of σ_{beam} in quadrature. The method described in [6], scaled by scan-dependent estimates of tropospheric activity [7], was used to calculate σ_{beam}.

Table 1. The rms of the delay variations of Fig. 1.

Scan	VLBI(t), ps	WVR(t), ps	$\Delta(t)$, ps	σ_{beam}, ps	Δ^*, ps
20	3.54	6.04	5.08	1.0	5.0
93	13.7	13.9	7.56	4.8	5.8

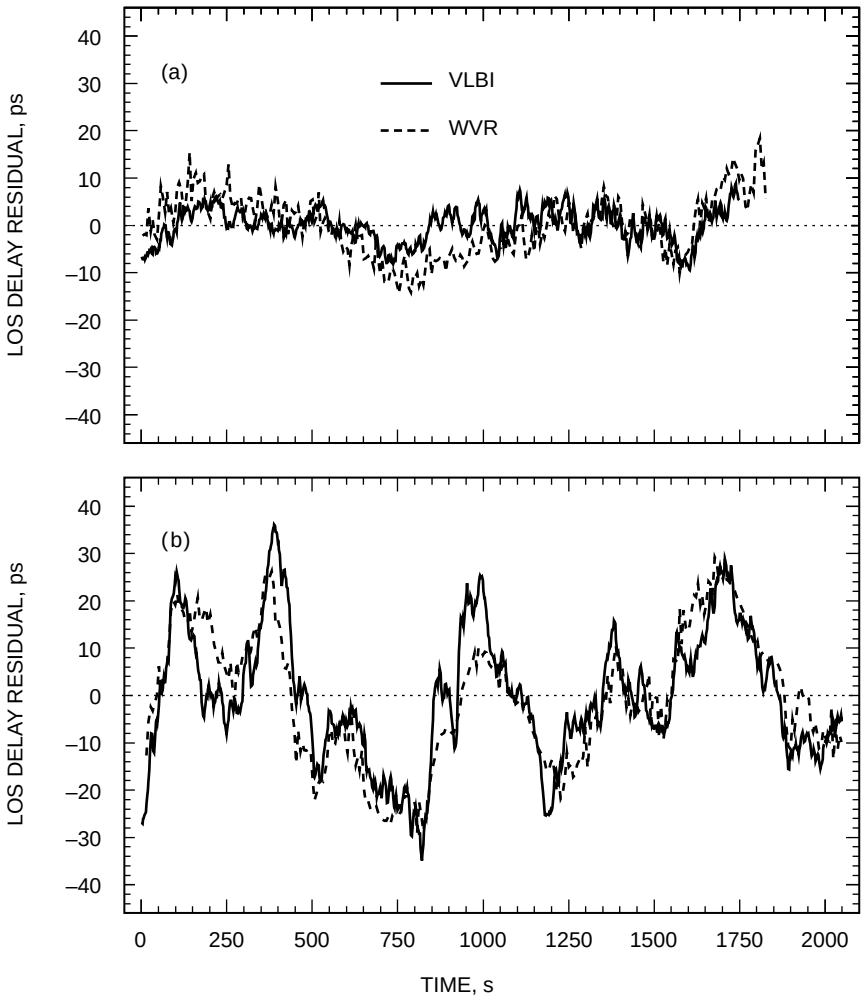

Fig. 1. Site-differenced, line-of-sight delay residuals for two long scans: (a) scan 20 and (b) scan 93. Both the VLBI and WVR delays are residuals with respect to linear fits.

For scan 20, the WVR time series has a much larger rms than the VLBI time series. However, the rms of $\Delta(t)$ is smaller than the WVR rms by $\sim$3 ps in quadrature, indicating that a 3-ps troposphere variation is common to the data but that the WVR instrument noise is large compared with the troposphere for this scan. In contrast, the WVR and VLBI time series for scan 93 show comparable variation and the rms of $\Delta(t)$ is significantly lower than the rms for both the VLBI and the WVR data, implying that 11–12 ps (rms) of tropospheric delay fluctuations have been removed by the calibration and confirming that the site-differenced delay residuals are troposphere dominated. Note that Δ^* is approximately the same for both scans, suggesting that the noise floor for the VLBI/WVR comparison technique with current instrumentation is $\sim$5–6 ps.

Figure 2 shows the Allan standard deviation of the delay $\sigma_\tau(T)$ as a function of time interval T for scan 93 for VLBI, WVR, and their difference, $\Delta(t)$. The VLBI and WVR data have similar Allan standard deviations, except for time scales $\lesssim$30 s, where thermal noise, characterized by the much steeper slope of the data, dominates the WVR spectrum. For thermal noise $\sigma_\tau(T) = \sqrt{3}N/T$, where N is the rms of the ensemble of noise-induced delay variations for a fixed integration time, in this case 6 s. From Fig. 2, $\sigma_\tau(10\text{ s}) \sim 7 \times 10^{-13}$ s/s $= 7 \times 10^{-12}$ s/T, implying $N \sim 4$ ps, approximately the same as Δ^* in Table 1.

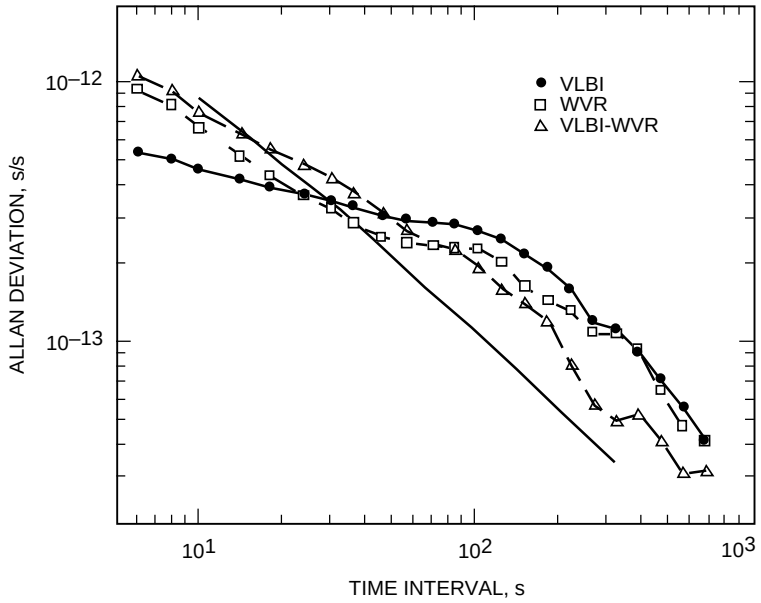

Fig. 2. Allan standard deviation of VLBI, WVR, and VLBI-WVR delay residuals for scan 93. The solid line is an estimate of the Allan deviation introduced because the VLBI and WVR antennas sampled different tropospheric volumes.

The VLBI data do not appear thermal noise limited (no increase in the magnitude of the slope to a value ≈ -1), even at $t \to 6$ s. For time intervals >100 s, the differenced data show a smaller Allan standard deviation than either the VLBI or WVR data separately, with the reduction being a factor of ≈ 2 for time intervals longer than $\sim$200 s. Also shown in Fig. 2 is the estimate of $\sigma_\tau(T)$ due to the tropospheric volume sampling differences, described above, between the WVR and DSN antennas. For time intervals longer than $\sim$200 s, the Allan deviation of $\Delta(t)$ is within a factor of ≈ 2 of this estimated error source.

Figure 3 shows the scan-averaged *zenith* group delay residuals of the VLBI and WVR data for the entire 13-h pass. The LOS residuals $\tau(\theta)$ have been mapped to zenith residuals τ_z to remove variations due solely to elevation angle differences between scans, using the mapping function $\tau_z = \tau(\theta) \sin\theta$. Figure 3(a) shows all 80 scans with valid data, while Fig. 3(b) shows the 30 scan subset for which the WVRs were copointing with the DSN antennas to better than 1 deg at both ends of the baseline. The VLBI LOS residuals were determined with respect to an a priori delay model [9] after the estimation of three parameters from the data, a clock difference τ_{cl}, a clock rate $\dot{\tau}_{cl}$, and a mean zenith troposphere difference $\overline{\tau}_z$. In order to compare the VLBI and WVR time series, the LOS WVR data had an equivalent linear model fitted to and subtracted from the data.

A strong correlation between VLBI and WVR estimates of site-differenced residual delays is evident in Fig. 3, particularly for the copointing data. Because a mean zenith troposphere has been removed, the variations represent the effects of tropospheric fluctuations. The VLBI/WVR correlation shows the ability of WVRs to provide a calibration on time scales ranging from the few minutes between individual scans to $\sim$7 hours (half the experiment duration; fluctuations on longer time scales would be absorbed by the fitting).

The WVR estimates of the LOS site-differenced delay fluctuations can be applied directly as a calibration before parameter estimation. The post-fit rms delay residuals are tabulated in Table 2 for different sets of estimated parameters, both for the full and copointing data sets. Results are given with and without the WVR calibration. Application of the calibration caused a dramatic reduction in the VLBI

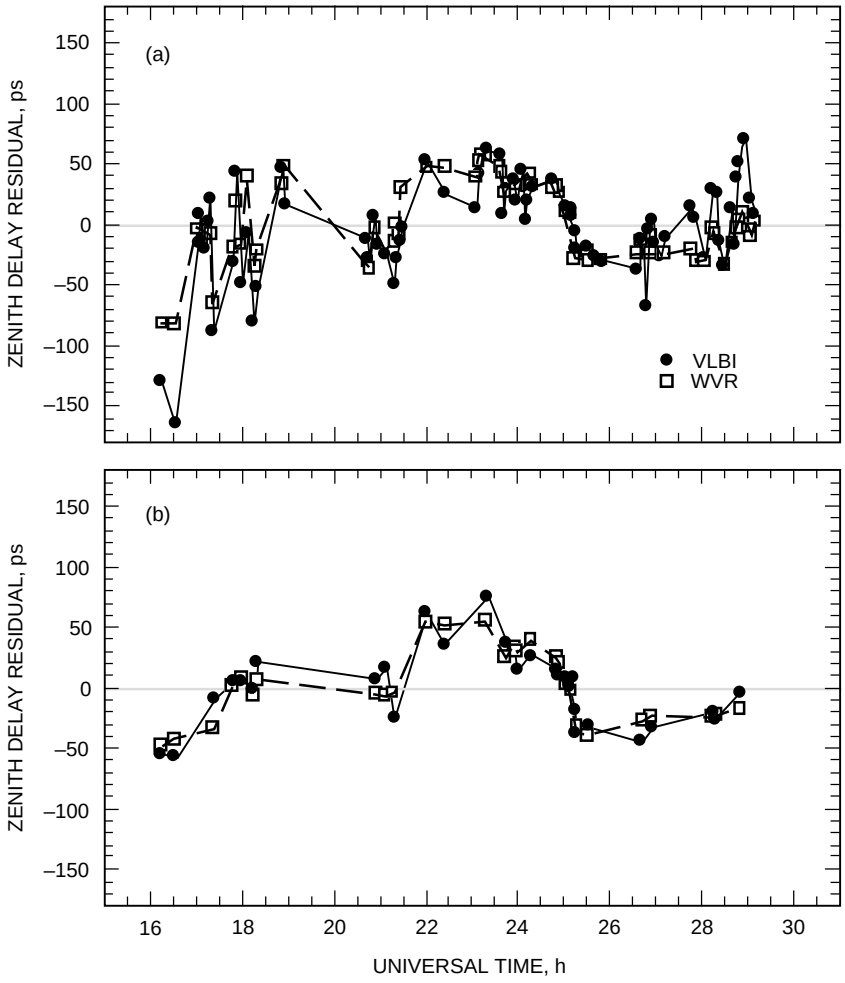

Fig. 3. Site-differenced *zenith* delay residuals for scan-averaged VLBI and WVR data: (a) valid scans and (b) copointing scans. Note the difference in time scale compared with Fig. 1. The top plot shows all 80 valid scans while the bottom plot shows only those 30 scans where the VLBI and WVR were copointing within 1 deg.

Table 2. The rms of the post-fit delay residuals after parameter estimation.

Estimated parameters	Valid (80 scans)		Copointing (30 scans)	
	No WVR, ps	WVR, ps	No WVR, ps	WVR, ps
$\tau_{cl}, \dot{\tau_{cl}}, \overline{\tau}_z$	106	52.0	43.8	16.9
$\tau_{cl}, \dot{\tau_{cl}}$	139	85.4	47.5	22.0
$\tau_{cl}, \overline{\tau}_z$	193	53.2	102	38.7
τ_{cl}	220	92.3	102	38.7

residuals in all cases. The calibration had the biggest impact when only τ_{cl} and $\overline{\tau}_z$ were estimated, as would be expected if the estimated clock rate $\dot{\tau_{cl}}$ also removed part of the linearly varying component of the troposphere. The largest single reduction in rms, a factor of 3.6, occurred when τ_{cl} and $\overline{\tau}_z$ were estimated for the full data set, in spite of a VLBI/WVR angular offset for numerous scans. This is because many low elevation angle scans ($\theta < 20$ deg) introduced large tropospheric effects for this data set. When only the 30 scans with copointed VLBI and WVR data were included, the reduction in rms residuals was a factor of from 2.2 to 2.6. A significant fraction of the rms delay residual of 16.9 ps for the copointing data can be accounted for by the 10.3-ps thermal noise in the VLBI group delay data type and ≈2.4 ps from WVR pointing error. For scan-averaged data, the WVR thermal noise is negligible.

Another possible error source for VLBI/WVR comparisons is *dry* delay fluctuations, due to temperature fluctuations in the components of dry air, which dominate astronomical "seeing" at optical wavelengths. Scaling up the delay structure function derived from seeing of a few arcseconds under the assumption of Kolmogorov turbulence suggests that dry delay fluctuations might account for one-third of the total observed fluctuations. However, measurements of the outer scale of turbulence in temperature fluctuations [1,2] suggest that dry fluctuations will saturate (and wet fluctuations will therefore dominate) for time scales larger than a few seconds during stable atmospheric conditions (e.g., at night) and for time scales larger than a few hundred seconds during large-scale daytime convection. Dry fluctuations may, therefore, explain part of the VLBI–WVR discrepancy within scan 93, but are probably not an important component of the uncalibrated scan-to-scan residuals shown in Table 2.

Acknowledgments

We thank C. Jacobs and C. Naudet for assistance with the experiment scheduling, and L. Skjerve, L. Tanida, R. Swindlehurst, and the DSS-13 crew for assistance with the observations.

References

[1] J. Barat and F. Bertin, "On the Contamination of Stratospheric Turbulence Measurements by Wind Shear," *Journal of the Atmospheric Sciences*, vol. 41, pp. 819–827, 1984.

[2] C. E. Coulman, J. Vernin, Y. Coqueugniot, and J. L. Caccia, "Outer Scale of Turbulence Appropriate to Modeling Refractive-Index Structure Profiles," *Applied Optics*, vol. 27, pp. 155–160, 1988.

[3] G. Elgered, "Tropospheric Radio-Path Delay From Ground-Based Microwave Radiometry," *Atmospheric Remote Sensing by Microwave Radiometry*, Chapter 5, edited by M. Janssen, New York: John Wiley, 1993.

[4] R. A. Hinder, "Observations of Atmospheric Turbulence With a Radio Telescope at 5 GHz," *Nature*, vol. 225, pp. 614–617, 1970.

[5] M. A. Janssen, "A New Instrument for the Determination of Radio Path Delay Due to Atmospheric Water Vapor," *IEEE Trans. Geosci. Remote Sensing*, vol. 23, pp. 485–490, 1985.

[6] R. P. Linfield and J. Z. Wilcox, "Radio Metric Errors Due to Mismatch and Offset Between a DSN Antenna Beam and the Beam of a Troposphere Calibration Instrument," *The Telecommunications and Data Acquisition Progress Report 42-114, April–June 1993*, Jet Propulsion Laboratory, Pasadena, California, pp. 1–13, August 15, 1993.

[7] R. P. Linfield, S. J. Keihm, L. P. Teitelbaum, S. J. Walter, M. J. Mahoney, R. N. Treuhaft, and L. J. Skjerve, "A Test of Water Vapor Radiometer-Based Troposphere Calibration Using VLBI Observations on a 21-Kilometer Baseline," *Radio Science*, vol. 31, pp. 129–146, 1996.

[8] S. T. Lowe, *Theory of Post-Block II VLBI Observable Extraction*, JPL Publication 92-7, Jet Propulsion Laboratory, Pasadena, California, 1992.

[9] O. J. Sovers and C. S. Jacobs, *Observation Model and Parameter Partials for the JPL VLBI Parameter Estimation Software "MODEST"—1994*, JPL Publication 83-38, Rev. 5, Jet Propulsion Laboratory, Pasadena, California, 1994.

[10] R. N. Treuhaft and G. E. Lanyi, "The Effect of the Dynamic Wet Troposphere on Radio Interferometer Measurements," *Radio Science*, vol. 22, pp. 251–265, 1987.

[11] S. J. Keihm, "Water Vapor Radiometer Measurements of the Tropospheric Delay Fluctuations at Goldstone Over a Full Year," *The Telecommunications and Data Acquisition Progress Report 42-122, April–June 1995*, Jet Propulsion Laboratory, Pasadena, California, pp. 1–11, August 15, 1995.
http://tda.jpl.nasa.gov/tda/progress_report/42-122/122J.pdf